Friction **11**(7): 1194–1211 (2023)
https://doi.org/10.1007/s40544-022-0648-z
ISSN 2223-7690
CN 10-1237/TH
RESEARCH ARTICLE

Bioinspired surface functionalization of biodegradable mesoporous silica nanoparticles for enhanced lubrication and drug release

Xiaowei MAO[1,2,†], Kexin CHEN[3,†], Yanlong ZHAO[2], Chunrong Xiong[1], Jing LUO[4], Yuguang WANG[5,*], Bo WANG[6,*], Hongyu ZHANG[2,*]

[1] *School of Chemical Engineering and Technology, Hainan University, Haikou 570228, China*

[2] *State Key Laboratory of Tribology, Department of Mechanical Engineering, Tsinghua University, Beijing 100084, China*

[3] *Peking University School of Nursing & National Engineering Laboratory for Digital and Material Technology of Stomatology, Beijing 100191, China*

[4] *Beijing Research Institute of Automation for Machinery Industry Co., Ltd., Beijing 100120, China*

[5] *Center of Digital Dentistry, Peking University School and Hospital of Stomatology & NHC Research Center of Engineering and Technology for Computerized Dentistry, Beijing 100081, China*

[6] *College of Chemical and Biological Engineering, Shandong University of Science and Technology, Qingdao 266590, China*

Received: 12 February 2022 / Revised: 02 April 2022 / Accepted: 08 May 2022

Abstract: Osteoarthritis is associated with the significantly increased friction of the joint, which results in progressive and irreversible damage to the articular cartilage. A synergistic therapy integrating lubrication enhancement and drug delivery is recently proposed for the treatment of early-stage osteoarthritis. In the present study, bioinspired by the self-adhesion performance of mussels and super-lubrication property of articular cartilages, a biomimetic self-adhesive dopamine methacrylamide–poly(2-methacryloyloxyethyl phosphorylcholine) (DMA–MPC) copolymer was designed and synthesized via free radical polymerization. The copolymer was successfully modified onto the surface of biodegradable mesoporous silica nanoparticles (bMSNs) by the dip-coating method to prepare the dual-functional nanoparticles (bMSNs@DMA–MPC), which were evaluated using a series of surface characterizations including the transmission electron microscope (TEM), Fourier transform infrared (FTIR) spectrum, thermogravimetric analysis (TGA), X-ray photoelectron spectroscopy (XPS), etc. The tribological test and *in vitro* drug release test demonstrated that the developed nanoparticles were endowed with improved lubrication performance and achieved the sustained release of an anti-inflammatory drug, i.e., diclofenac sodium (DS). In addition, the *in vitro* biodegradation test showed that the nanoparticles were almost completely biodegraded within 10 d. Furthermore, the dual-functional nanoparticles were biocompatible and effectively reduced the expression levels of two inflammation factors such as interleukin-1β (IL-1β) and interleukin-6 (IL-6). In summary, the surface functionalized nanoparticles with improved lubrication and local drug release can be applied as a potential intra-articularly injected biolubricant for synergistic treatment of early-stage osteoarthritis.

Keywords: surface functionalization; phosphorylcholine coating; mesoporous silica nanoparticles; hydration lubrication; osteoarthritis

1 Introduction

Osteoarthritis is a typical chronic joint disease featured with severe articular cartilage wear and joint capsule inflammation [1–5]. It is caused by the irreversible reduction in the lubrication performance of synovial

† Xiaowei MAO and Kexin CHEN contributed equally to this work.

* Corresponding authors: Yuguang WANG, E-mail: wangyuguang@bjmu.edu.cn; Bo WANG, E-mail: wb@sdust.edu.cn; Hongyu ZHANG, E-mail: zhanghyu@tsinghua.edu.cn

fluid and progressive degradation of cartilage matrix, such as the loss of glycosaminoglycan, occurrence of tissue fibrosis, and increased surface roughness, which ultimately results in the development of osteoarthritis [6–10]. An amount of people worldwide suffer from osteoarthritis every year, and it has become one of the major diseases that affects the quality of life for the patients in orthopedics [11, 12]. Currently, artificial joint replacement is recommended in clinics to treat end-stage osteoarthritis, but the patients often experience aseptic loosening of the implants after the surgery, which can accelerate the production of wear debris from the femoral component and eventually results in the functional failure of this surgery [13]. On the other hand, the treatment for early-stage osteoarthritis is usually oral administration of some common anti-inflammatory drugs, such as ibuprofen, meloxicam, etc. However, as there are insufficient blood vessels in the articular cartilage, the drugs cannot reach the joint cavity through blood circulation effectively. Therefore, it is difficult for these anti-inflammation drugs to be absorbed, making the therapeutic effect of osteoarthritis treatment usually unsatisfactory [14, 15]. Based on the above considerations, the local intra-articular injection of nanocarriers with pre-encapsulated anti-inflammatory drugs into the joint represents an alternative strategy. The intra-articular drug delivery offers the advantages of increased local drug concentration, reduced systemic exposure, and fewer adverse effects compared with previous treatment of oral drug administration [16]. Therefore, the development of a novel protocol for achieving enhanced joint lubrication and local drug delivery is of great importance for the treatment and prevention of early-stage osteoarthritis.

The natural articular cartilage is a well-known system with super-lubrication property, and the cartilage matrix consists of a large number of collagen fibers and proteoglycans. Articular cartilage functions together with the synovial fluid in the joint cavity to ensure that the joint can bear high physiological pressures with an extremely small coefficient of friction (COF, 0.001–0.01) [17–21]. The excellent lubrication behavior of articular cartilage is owing to a synergistic interaction of the biomolecules including hyaluronic acid, aggrecan, proteoglycan, and phosphatidylcholine, and the lubrication mechanism is developed by Klein [22] to be hydration lubrication. On the other hand, among the different kinds of drug nanocarriers, biodegradable mesoporous silica nanoparticles (bMSNs) are a commonly used inorganic nanomaterial with superior advantages such as large specific surface area, adjustable pore size, good biocompatibility, easy surface modification, and biodegradability [23–25]. To enhance the lubrication performance of bMSNs, a surface modification method can be employed to graft lubrication molecules onto the surface of the nanoparticles. Poly(2-methacryloyloxyethyl phosphorylcholine) (PMPC) is a typical polymer with similar zwitterionic charges (i.e., $N^+(CH_3)_3$ and PO_4^-) as the phosphatidylcholine lipids in articular cartilage, which can attract as many as up to 15 water molecules around the phosphorylcholine groups. Accordingly, the tenacious hydration layer formed between two contact surfaces results in a significant reduction in the COF value even at high contact pressures [26]. Nowadays, similar zwitterionic polymers have been grafted onto hyaluronic acid [27], mesoporous silica nanoparticles [28, 29], arginine–glycine–aspartic acid [30], and other materials in order to improve the lubrication performance of the material. However, it is considered that a facile surface functionalization strategy has not been investigated to modify bioinspired coating onto the surface of bMSNs in previous studies.

Surface coating and modification technology have been shown to reduce friction and enhance lubrication for a wide range of materials [31]. Based on the research reported by Lee et al. [32], the catechol and amine groups in the mussel proteins can self-adhere to almost all types of inorganic and organic substrates. As a consequence, dopamine, a dihydroxyphenylalanine derivative with similar adhesion behavior to that of mussels, has attracted considerable attention in recent years [33]. Dopamine is chemically active for further synthesis of dopamine-based self-adhesive materials, and there are a large number of hydrogen bonding between donor/acceptor groups that can form relatively strong interactions during the deposition process onto the surface of the substrates [34]. Herein, bioinspired from the self-adhesion performance of mussel and super-lubrication property of articular

cartilage, we developed a biomimetic self-adhesive copolymer via free radical polymerization employing dopamine methacrylamide–poly(2-methacryloyloxyethyl phosphorylcholine) (DMA–MPC). As displayed in Fig. 1, the DMA–MPC copolymer was coated on the surface of bMSNs due to the formation of hydrogen bonds between the hydroxyl groups in bMSNs and the phenolic hydroxyl groups in DMA–MPC, and afterwards an anti-inflammation drug of diclofenac sodium (DS) was loaded into the nanoparticles to prepare bMSNs@DMA–MPC–DS. Consequently, the dual-functional nanoparticles not only greatly enhanced lubrication property but also were endowed with a sustained drug delivery to achieve the anti-inflammation propose. It was anticipated that the nanoparticles developed herein with the performances of improved lubrication and drug release might be served as a potential intra-articular agent for early-stage osteoarthritis treatment.

2 Materials and methods

2.1 Materials and reagents

Cetyltrimethylammonium chloride (CTAC) solution and cyclohexane were purchased from Senrise Technology Co., Ltd., Anqing, China. Tetraethyl orthosilicate (TEOS), triethanolamine (TEA), DS, and hydrochloric acid were purchased from J&K Scientific Co., Ltd., Beijing, China. 2,2'-azodiisobutyronitrile (AIBN) and sodium pyroborate were purchased from Aladdin Bio-Chem Technology Co., Ltd., Shanghai, China. Deuterated water (D_2O) was purchased from InnoChem Co., Ltd, Beijing, China. Tris(hydroxymethyl)aminomethane hydrochloride (Tris-HCl) buffer (pH = 8.5) and simulated body fluid (SBF, pH = 6.0) were purchased from Beijing Solarbio Science & Technology Co., Ltd., Beijing, China. Methanol and phosphate buffered saline (PBS) solution (pH = 7.4) at a concentration of 10 mM were purchased from Shanghai Titan Scientific Co., Ltd., Shanghai, China. Thin carbon support film was purchased from Beijing Zhongjingkeyi Technology Co., Ltd., Beijing, China. 2-MPC was purchased from Joy-Nature Corp., Nanjing, China. Ethyl acetate, magnesium sulfate, and petroleum ether were purchased from Modern Oriental Technology Development Co., Ltd., Beijing, China. Lipopolysaccharide (LPS) was purchased from Sigma, USA. Live & dead viability and cytotoxicity assay kit was purchased from Nanjing Keygen Biotech Co., Ltd., Nanjing, China. Alpha-minimum essential medium (α-MEM) was purchased from Thermo Fisher Scientific Co., Ltd., Beijing, China. The enzyme-linked immunosorbent assay

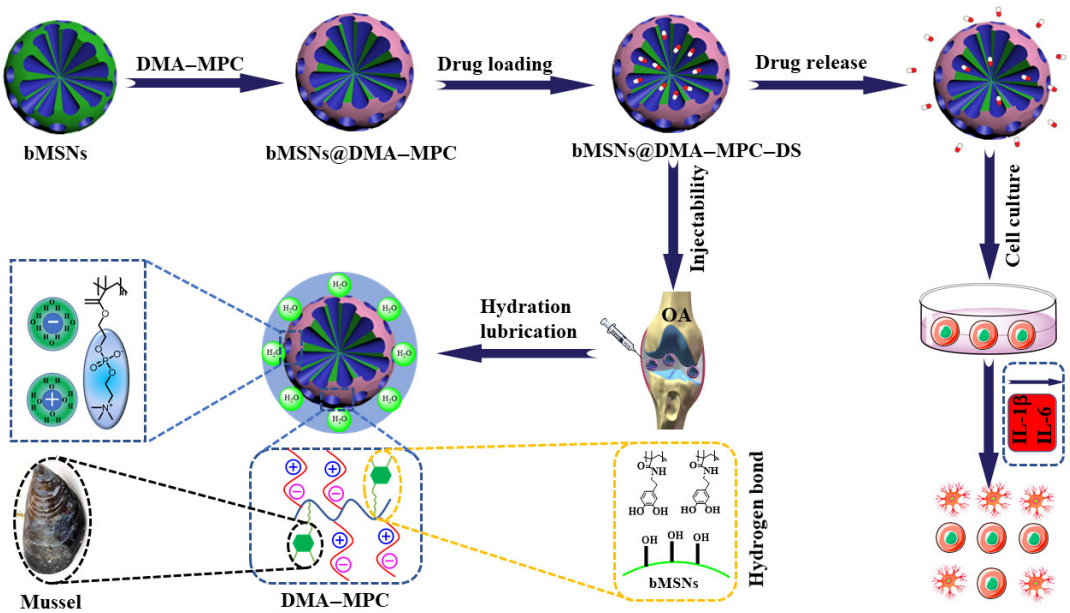

Fig. 1 Schematic image exhibiting the preparation of dual-functional nanoparticles of bMSNs@DMA–MPC–DS with improved lubrication and sustained drug release for early-stage osteoarthritis treatment.

(ELISA) kit was purchased from Beijing 4A Biotech Co., Ltd., Beijing, China. Fetal bovine serum was purchased from Life Technologies Pty Ltd., Australia. Cell Counting Kit-8 (CCK-8) was purchased from New Cell & Molecular Biotech Co., Ltd., Suzhou, China.

2.2 Synthesis of bMSNs

The synthesis of bMSNs was based on the procedure as described in the previous study [35]. Briefly, CTAC (120 mL), TEA (0.9 g), and deionized water (180 mL) were mixed and stirred continuously for 1 h at 60 °C. Subsequently, a mixture of TEOS (5 mL) and cyclohexane (95 mL) was added, and the solution was further stirred at 60 °C for 62 h. The bMSNs containing CTAC template were collected via centrifugation (8,000 r/min), followed by condensation and reflux in acidic methanol for 24 h at 60 °C, and finally dried in vacuum in order to obtain the nanoparticles.

2.3 Synthesis of DMA–MPC

The copolymer of DMA–MPC was prepared according to the procedure as described in our previous study [33]. Briefly, a mixture of DMA (0.2 g), MPC (0.8 g), and triggering agent AIBN (3 mg) were dissolved in N,N-dimethylformamide (50 mL) and then stirred continuously in an atmosphere of N_2 for 24 h at 65 °C. The product was dialyzed in the dialysis bags (molecular weight cutoff: 1,000 Da) for 3 d and finally lyophilized to obtain the white powder. Similarly, the DMA–MPC copolymers with various mass ratios (DMA:MPC = 1:1 and 4:1) were also prepared.

2.4 Preparation of bMSNs@DMA–MPC

The synthesis of bMSNs@DMA–MPC was based on the method previously reported in our study [36]. Briefly, DMA–MPC copolymer (40 mg) and bMSNs solid powder (20 mg) were homogeneously dispersed in Tris-HCl (10 mL) and stirred continuously for 24 h at room temperature. The product was obtained via centrifugation and washed by a large amount of deionized water to remove the unattached copolymer on the surface. Finally, the solid powder of bMSNs@DMA–MPC was freeze-dried in a freeze-dryer.

2.5 Material characterizations

The ^{1}H nuclear magnetic resonance (NMR) spectrum for the copolymer of DMA–MPC was recorded using a spectrometer (AVANCE III, Bruker, Germany) with D_2O as the solvent. The molecular weight distribution of the DMA–MPC copolymer with different ratios was obtained utilizing a gel permeation chromatography (GPC) device (Viscotek TDA305max, Malvern Instruments, UK) at the flow rate of 0.7 mL/min with sodium nitrate (0.1 M) as the diluent. The surface feature of bMSNs and bMSNs@DMA–MPC was observed by the transmission electron microscope (TEM; HT7800, Hitachi, Japan) operated at the acceleration voltage of 80 kV. Prior to the TEM measurement, the powder nanoparticles were uniformly dispersed in deionized water, and dried on a Cu mesh. The zeta potentials of bMSNs, DMA–MPC, and bMSNs@DMA–MPC associated with the hydrodynamic diameters of the nanoparticles were analyzed using a particle size analyzer (Zetasizer Nano ZS90, Malvern Instruments, UK), which was calculated by the dynamic light scattering (DLS) technique. The Fourier transform infrared (FTIR) spectra for bMSNs and bMSNs@DMA–MPC were recorded via the FTIR spectrometer (Vertex 70, Bruker, Germany) at a wavelength range of 600–4,000 cm^{-1}. The thermogravimetric analyses of bMSNs and bMSNs@DMA–MPC were evaluated using a thermogravimetric analysis (TGA) instrument (Q5000IR, TA Instruments, USA) at the heating rate of 10 °C/min over a temperature range of 25–820 °C. The values of pore volume and specific surface area for bMSNs and bMSNs@DMA–MPC were obtained using a nitrogen adsorption–desorption system (NOVA 4000, Quantachrome Instruments, USA) by the Barrett–Joyner–Halenda (BJH) and Brunauer–Emmett–Teller (BET) models. The surface elemental compositions for the bMSNs and bMSNs@DMA–MPC nanoparticles were examined employing an X-ray photoelectron spectrometer (PHI5300, Physical Electronics, USA).

2.6 Rheological test

The rheological property of the bMSNs@DMA–MPC nanoparticles was tested utilizing a Physica MCR302 rheometer (Anton Paar, Austria), which was equipped with a module of cone-and-plate configuration. Briefly,

the aqueous suspensions of bMSNs@DMA–MPC (1:4) nanoparticles at various concentrations (1, 2, and 5 mg/mL) were prepared, and 1 mL of the aqueous suspension was added drop by drop on the surface of the plate. The range of shear rate was set from 10 to 8,000 s^{-1}, and the shear stress vs. shear rate curve and viscosity vs. shear rate curve were recorded under the shearing mode.

2.7 Tribological test

The tribological test was conducted to examine the lubrication behavior of the bMSNs and bMSNs@DMA–MPC nanoparticles employing a universal material tester (UMT-5, Centre for Tribology Inc., USA) under a reciprocating mode (amplitude of oscillation: 4 mm). The aqueous suspensions of bMSNs and bMSNs@DMA–MPC (1:4, 1:1, and 4:1) with various concentrations (1, 2, and 5 mg/mL) were prepared and tested. The upper specimen was a polytetrafluoroethylene (PTFE) ball (diameter: 8 mm), and the lower specimen was a highly-polished Ti6Al4V sheet, which slid against the PTFE during the test. The tribological tests were conducted under different loadings (1, 2, and 3 N) and different reciprocating frequencies (1, 2, and 3 Hz), and each test was lasted for 10 min. The final COF, which was assigned as the lateral loading divided by the normal loading, was calculated as the average of three measurements obtained from various locations on the Ti6Al4V sheet. Additionally, the Hertz contact theory was used to calculate the apparent maximum contact pressure by Eq. (1) for ball-on-flat contact.

$$P = \frac{1}{\pi}\sqrt[3]{\frac{6F}{\left(\frac{1-\mu_1^2}{E_1}+\frac{1-\mu_2^2}{E_2}\right)^2 R^2}} \tag{1}$$

In Eq. (1), P was the contact pressure (MPa), F was the applied loading (1, 2, and 3 N), R was the radius of the PTFE ball (4 mm), μ_1 and μ_2 were the Poisson's ratios of PTFE (0.3) and Ti6Al4V (0.3), respectively, and E_1 and E_2 were the elastic moduli of PTFE (0.5 GPa) and Ti6Al4V (110 GPa), respectively. Accordingly, the maximum contact pressures were calculated as 15.4 MPa (1 N), 19.3 MPa (2 N), and 22.1 MPa (3 N). The comparison of lubrication performance between the bMSNs and bMSNs@DMA–MPC nanoparticles was further examined by the tribological test with extended time duration (30 min) under a concentration of 1 mg/mL, a contact pressure of 22.1 MPa, and a reciprocating frequency of 1 Hz. The surface morphology of the wear zone on the Ti6Al4V surface was investigated utilizing an optical interferometer (Nexview, ZYGO, USA) after the tribological test.

2.8 *In vitro* drug loading and release test

The *in vitro* drug loading and release test was performed to examine the sustained drug release property of the nanoparticles. Briefly, bMSNs@DMA–MPC (1:4, 60 mg) and DS (10 mg) were sonicated and homogeneously dispersed in PBS (10 mL), and then stirred for 24 h at room temperature. The nanoparticles were collected via centrifugation for 10 min (8,000 r/min), washed sufficiently with deionized water, and freeze-dried to obtain the drug-loaded nanoparticles (i.e., bMSNs@DMA–MPC–DS). Additionally, the standard curve was previously measured by collecting the absorbance value of DS with a range of concentrations (0.01, 0.02, 0.03, 0.04, and 0.05 mg/mL) in PBS utilizing a spectrophotometer (UV-8000, Metash Instruments, China) at the wavelength of 276 nm. The equation of the fitted standard curve was $Y = 20.218X - 0.0095$, where Y and X were the absorbance and concentration of the solution, respectively. The drug loading capacity (LC) as well as encapsulation efficiency (EE) of the two nanoparticles was calculated based on Eqs. (2)–(4):

$$\mathrm{LC}_{\mathrm{bMSNs}} = \frac{\text{Mass of encapsulated drug}}{\text{Mass of drug-loaded bMSNs}} \times 100\% \tag{2}$$

$$\mathrm{LC}_{\mathrm{bMSNs@DMA-MPC}} = \frac{\text{Mass of encapsulated drug}}{\text{Mass of drug-loaded bMSNs@DMA}-\text{MPC}} \times 100\% \tag{3}$$

$$\mathrm{EE} = \frac{\text{Mass of encapsulated drug}}{\text{Mass of added drug}} \times 100\% \tag{4}$$

The drug-loaded nanoparticles without surface coating (bMSNs–DS) were prepared similarly based on the above procedure.

The drug release behavior of DS from the nanoparticles was investigated by a dialysis bag

diffusion test, which was lasted for a duration of 80 h. Briefly, bMSNs–DS (30 mg) and bMSNs@DMA–MPC (1:4)–DS (30 mg) were sonicated and uniformly dispersed in PBS (6 mL). Afterwards, the suspensions (2 mL) of bMSNs–DS and bMSNs@DMA–MPC (1:4)–DS were packed into a dialysis bag with a molecular weight cutoff of 8,000–10,000 and immersed in 98 mL of PBS to form the 100 mL drug release solution for dialysis at 37 °C. At pre-determined time intervals, the medium (2 mL) was removed from the solution outside the dialysis bag, and then fresh PBS (2 mL) was supplemented. The absorbance value of the removed solution was measured at a wavelength of 276 nm using the spectrophotometer, and finally the cumulative drug release vs. time curve was plotted.

2.9 *In vitro* biodegradation test

The *in vitro* biodegradation test of the bMSNs and bMSNs@DMA–MPC nanoparticles was performed based on the procedure reported in the previous study [37]. Briefly, 5 mg of bMSNs and 5 mg bMSNs@DMA–MPC (1:4) were uniformly dispersed in 20 mL SBF and then incubated in a shaker for 0, 1, 5, and 10 d at 37 °C. At predetermined time intervals, 100 μL of the aqueous suspensions were removed, and the nanoparticles were collected via centrifugation. An equal volume of fresh SBF was supplemented to the original solution, and the degradation of the nanoparticles was characterized using the TEM for morphological observation. In addition, the lubrication performance of the bMSNs and bMSNs@DMA–MPC (1:4) nanoparticles incubated with SBF at different time intervals was investigated using the universal materials tester. The tribological test was performed under the following conditions: concentration (1 mg/mL), reciprocating frequencies (1 Hz), and contact pressure (22.1 MPa), each for a duration of 10 min.

2.10 *In vitro* biocompatibility

The cytotoxicity and live/dead staining assays were performed to evaluate the *in vitro* biocompatibility of the bMSNs and bMSNs@DMA–MPC nanoparticles to determine whether the nanoparticles were suitable for intra-articular application [38, 39]. MC3T3-E1 cells were used, and cytotoxicity was assessed by CCK-8 and live/dead cell staining assays. Briefly, the MC3T3-E1 cells were cultured in α-MEM, which was supplemented with fetal bovine serum (10%). The cells were kept in an incubator maintaining at 37 °C, 5% CO_2, and 95% humidity. The MC3T3-E1 cells were passaged every 3 d, and the culture medium was replaced everyday. The MC3T3-E1 cells were incubated in 96-well plates at a density of 3×10^3 cell/well for 24 h, followed by the addition of bMSNs and bMSNs@DMA–MPC (1:4). The cells were cultured with various concentrations of bMSNs and bMSNs@DMA–MPC (1:4) (0.05–1.0 mg/mL) for 24 h in order to examine the effect of concentration on cytotoxicity. Afterwards, the concentration of 0.05 mg/mL was selected as the value to investigate the cytotoxicity of the nanoparticles on 1, 3, and 5 d. Cytotoxicity was evaluated by the CCK-8 assay. Generally, 100 μL of the CCK-8 solution (10%) was added to each well, and then cultured for 2 h. The absorbance value of the solution was recorded utilizing a microplate reader (FLUOstar Omega, BMG LABTECH, Germany) at the wavelength of 450 nm. The viability of the MC3T3-E1 cells after culturing with 0.05 mg/mL of bMSNs and bMSNs@DMA–MPC (1:4) for 1, 3, and 5 d was examined employing the live/dead cell staining kit. Briefly, the MC3T3-E1 cells were incubated in 6-well plates at a density of 3×10^3 cell/well. Following incubation with 0.05 mg/mL of bMSNs and bMSNs@DMA–MPC (1:4) for 1, 3, and 5 d, the cells were stained by the cell dye for 15 min, and then imaged utilizing a laser scanning confocal microscope (LSM-800, Zeiss, Germany).

2.11 Anti-inflammation evaluation

The anti-inflammatory test of the bMSNs and bMSNs@DMA–MPC nanoparticles was performed based on the procedure reported in the previous study [40]. The inflammation factors secreted by the macrophages were detected using the ELISA. Briefly, macrophages (RAW 264.7) were seeded in 6-well plates with a density of 1×10^5 cell/well, and then incubated overnight. The cell culture medium was removed after induction of activation by LPS. Roswell park memorial institute (RPMI) medium 1640 containing the same concentrations of the

nanoparticles including bMSNs, bMSNs@DMA–MPC (1:4), bMSNs–DS, bMSNs@DMA–MPC (1:4)–DS, and the same volume of medium 1640 were used to incubate with the activated macrophages. After incubation for 24 h, the cell supernatant was collected following centrifugation, and the levels of the inflammation factors, such as interleukin-1β (IL-1β) and interleukin-6 (IL-6), were measured using the ELISA kit, and the controls without bMSNs, bMSNs@DMA–MPC (1:4), bMSNs–DS, and bMSNs@DMA–MPC (1:4)–DS were tested for comparison.

2.12 Statistical analysis

The quantitative data were shown as average value ± standard deviation, and the similar independent experiments were performed repeatedly for at least three times in order to validate the results. Statistical analysis was conducted by the GraphPad Prism software (GraphPad Software Inc., USA), and the statistical significance was indicated as $^{*}P < 0.05$.

3 Results and discussion

3.1 Synthesis and characterizations of DMA–MPC

The ^{1}H NMR spectra of the DMA–MPC copolymer with different mass ratios are shown in Fig. 2(a). The chemical shifts at 7.85 and 6.79 ppm are attributed to the signals in DMA, and the chemical shift at 3.11 ppm is assigned to the signals in MPC [41, 42]. The molecular weight (M_w) for the copolymer of DMA–MPC with various mass ratios is displayed in Fig. 2(b), which is calculated to be 855.834, 660.706, and 760.568 kDa. The results of NMR and GPC demonstrate that the DMA–MPC copolymer has been synthesized successfully via free radical polymerization.

3.2 Synthesis and characterizations of bMSNs@DMA–MPC

The representative TEM images of bMSNs and bMSNs@DMA–MPC (1:4) are shown in Figs. 3(a) and 3(b), respectively. The morphology of the nanoparticles indicates that bMSNs and bMSNs@DMA–MPC are dendritic in shape with uniform size and good

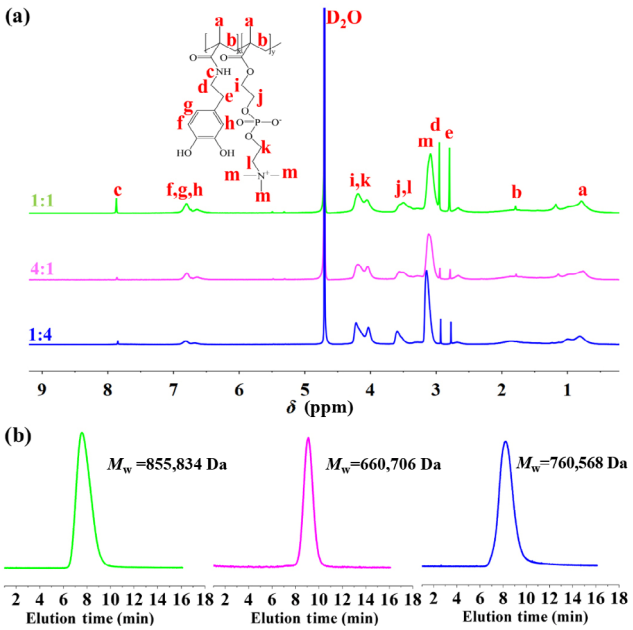

Fig. 2 Characterizations of the DMA–MPC copolymer with various mass ratios: (a) ^{1}H NMR spectra and (b) GPC chromatogram analysis.

dispersion, and the average size is about 200 nm. After modification by the DMA–MPC copolymer, the surface of bMSNs@DMA–MPC becomes slightly blurred [43]. Figure 3(c) shows the zeta potential measurements of the two nanoparticles. The bMSNs have a negative zeta potential value of −22.1 mV, which is attributed to the presence of a large number of negatively-charged hydroxyl groups on the surface. The zeta potential values of DMA–MPC (1:4) and bMSNs@DMA–MPC (1:4) are −6.32 and −36.3 mV, respectively, indicating that following surface coating, the nanoparticles are still negatively charged [44]. It is considered that the nanoparticles can maintain high colloidal stability when the zeta potential is below −30 mV [45]. The hydrodynamic diameters of the two nanoparticles are shown in Figs. 3(d) and 3(e), where the values for bMSNs and bMSNs@DMA–MPC (1:4) are 274.7 and 518.4 nm, respectively. The hydrodynamic diameter of bMSNs@DMA–MPC is larger than that of bMSNs due to the surface coating of the DMA–MPC copolymer, and these values are higher than the corresponding measurements from the TEM images owing to the hydration effects of the zwitterionic polymers [46]. Figure 3(f) demonstrates the FTIR spectra of the nanoparticles. Compared with the spectrum of bMSNs, the peak at 3,345 cm^{-1} for

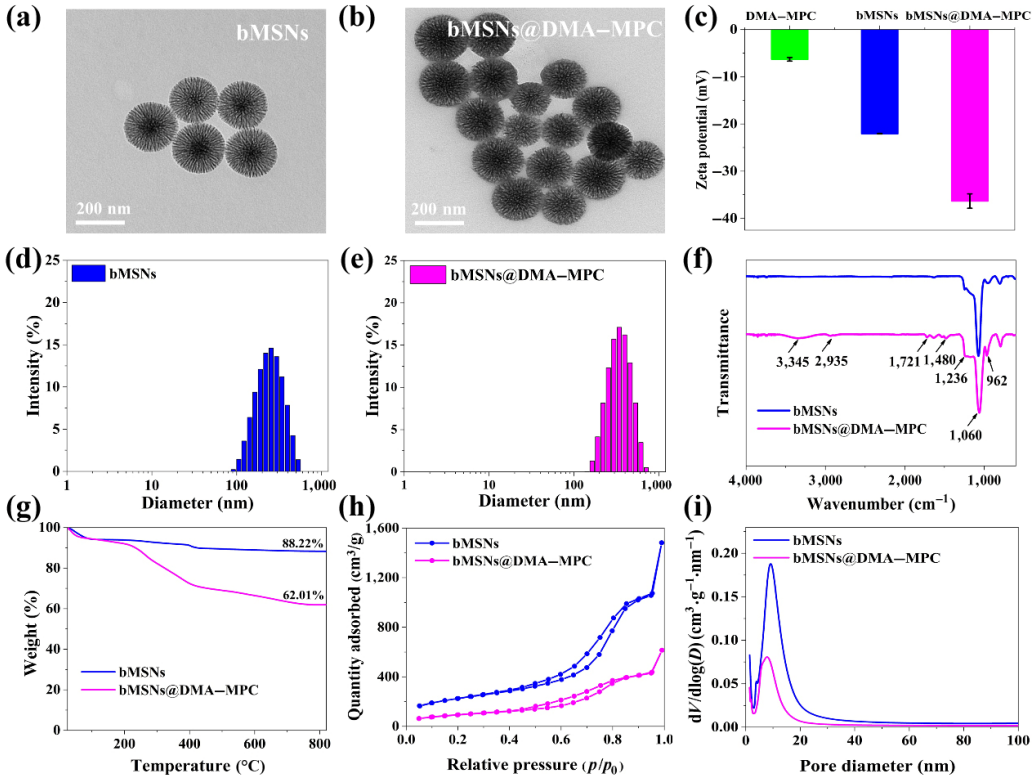

Fig. 3 Characterizations of the bMSNs and bMSNs@DMA–MPC (1:4) nanoparticles. TEM images of (a) bMSNs and (b) bMSNs@DMA–MPC. (c) Zeta potentials of DMA–MPC, bMSNs, and bMSNs@DMA–MPC. Histogram distributions showing the hydrodynamic diameters for (d) bMSNs and (e) bMSNs@DMA–MPC in aqueous medium at 25°C. (f) FTIR spectra, (g) TGA curves, (h) N_2 adsorption–desorption isotherms, and (i) pore size distributions of bMSNs and bMSNs@DMA–MPC.

bMSNs@DMA–MPC (1:4) belongs to the stretching vibration of –NH or phenyl –OH in DMA–MPC [47]. The peak at 2,935 cm^{-1} corresponds to the stretching vibration absorption band of alkane hydrogen. Additionally, the peaks at 1,721 and 1,480 cm^{-1} are assigned to the stretching vibration of the ester group and the –CH in the quaternary ammonium group, respectively [48]. The absorption band of Si–O–Si is located at 1,060 cm^{-1}, and the stretching vibrations of P=O and P–O are detected at 1,236 and 962 cm^{-1}, respectively [28]. The above surface characterizations indicate that the DMA–MPC copolymer has been modified successfully on the surface of the nanoparticles.

To examine the weight percentage of the DMA–MPC copolymer in the nanoparticles, the TGA is performed for bMSNs and bMSNs@DMA–MPC (1:4), and the results are shown in Fig. 3(g). It is clear from the TGA curves of the nanoparticles that the weight loss of bMSNs is 11.78%, which is probably due to the removal of the adsorbed water and the dehydrated hydroxyl groups on the surface [49]. The weight loss of bMSNs@DMA–MPC (1:4) is 37.99%, and therefore the content of the DMA–MPC copolymer coating in bMSNs@DMA–MPC is calculated as about 29.71%. Nitrogen adsorption/desorption isotherm is used to characterize the mesoporous properties of the nanoparticles, and the results of typical adsorption/desorption isotherm and pore size distribution of bMSNs and bMSNs@DMA–MPC (1:4) are shown in Figs. 3(h) and 3(i), respectively. The isotherms of the two nanoparticles can be categorized as Type IV pattern, which is typical of mesoporous materials [37]. Based on the BJH and BET models, the specific surface area and pore volume of bMSNs are 866.143 m^2/g and 2.299 mL/g, respectively, which significantly decreases to 419.178 m^2/g and 0.978 mL/g for bMSNs@DMA–MPC. Additionally, the average pore size of bMSNs is approximately 9.487 nm, which reduces to 7.760 nm for bMSNs@DMA–MPC. The changes in pore size, pore volume, and specific surface area are summarized in Table 1, and the results further indicate the presence

Table 1 Structural properties of bMSNs and bMSNs@DMA–MPC nanoparticles.

Nanoparticle	S_{BET}[1] (m^2/g)	V_p[2] (mL/g)	Pore size[3] (nm)	DLS[4] (nm)
bMSNs	866.143	2.299	9.487	274.7
bMSNs @DMA–MPC	419.178	0.978	7.760	518.4

[1] Specific surface area;
[2] Pore volume;
[3] Average pore size;
[4] Hydrodynamic diameter.

of DMA–MPC copolymer on the surface of the nanoparticles, covering the mesopores and accordingly reducing the mesopore-related parameters [50].

To evaluate the surface elemental compositions of the nanoparticles, the X-ray photoelectron spectroscopy (XPS) analysis of bMSNs and bMSNs@DMA–MPC (1:4) is further conducted, and the result is shown in Fig. 4. The binding energies of Si 2p, Si 2s, and O 1s in bMSNs are observed at 102.4, 152.8, and 531.9 eV, respectively. Compared with the spectrum of bMSNs, the new signal peaks are observed for bMSNs@DMA–MPC at 131.8 eV (P 2p), 191.2 eV (P 2s), and 400.8 eV (N 1s) [17], which is attributed to the presence of the DMA–MPC copolymer on the surface of the nanoparticles. Additionally, the intensity of the signal peaks for Si 2p and Si 2s is reduced, following the modification of the surface coating [51], as displayed in Fig. 4(a). Furthermore, the deconvolution analysis of N 1s, P 2p, and C 1s for the bMSNs and bMSNs@DMA–MPC nanoparticles is demonstrated in Figs. 4(b)–4(d). Clearly, no characteristic signal peaks of N 1s and P 2p are detected for the spectra of bMSNs. However, there are two obvious signal peaks of N 1s for the spectrum of bMSNs@DMA–MPC. The binding energy at 398.5 eV corresponds to the –NHCO– group in DMA, and the one at 400.8 eV is attributed to the $-N^+(CH_3)_3$ group in MPC. In addition, the signal peak of P 2p with the binding energy at 132.7 eV originates from the $-OPOCH_2-$ group in MPC. Regarding the analysis of C 1s narrow spectrum for the nanoparticles, only two signal peaks are observed for bMSNs, and the binding energies at 284.6 and 287.2 eV are assigned to C–C/C–Si and C–O groups, respectively [52]. For the spectra of bMSNs@DMA–MPC, two new signal peaks are detected with the binding energies at 285.7 and 288.6 eV, which belong to the C–N group in DMA [42] and the C=O group of the amide bond in DMA and ester bond in PMPC, respectively [33]. The above analysis of XPS spectra provides further evidence for confirming the successful modification of the DMA–MPC copolymer on the surface of the nanoparticles.

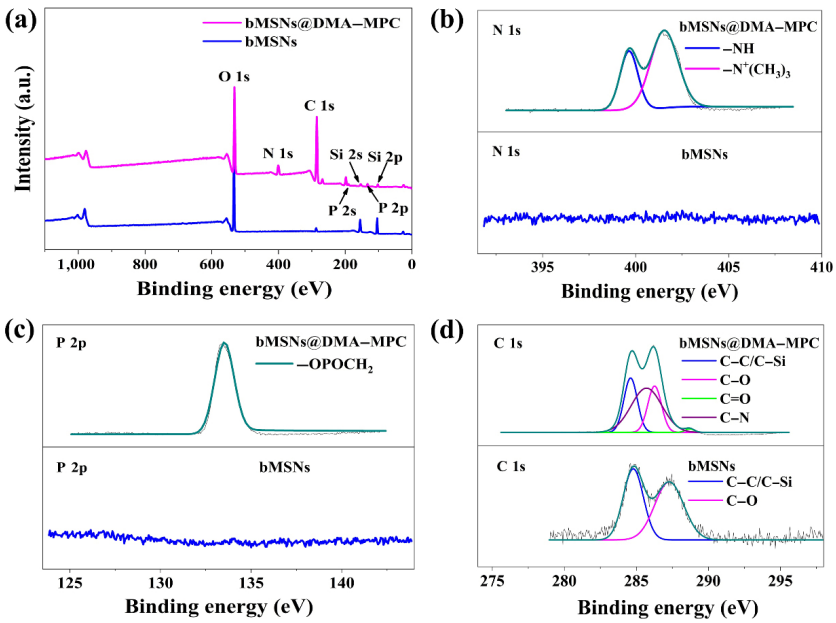

Fig. 4 XPS spectra of bMSNs and bMSNs@DMA–MPC (1:4) nanoparticles. (a) Comparison of the XPS spectra between the nanoparticles. Deconvolution analysis of the nanoparticles for (b) N 1s, (c) P 2p, and (d) C 1s.

3.3 Rheological property and lubrication performance

An intra-articular injection of biolubricants is an effective method commonly used for early-stage osteoarthritis treatment [16, 53], consequently the rheological property and lubrication behavior of the nanoparticles are investigated in the following experiments. Figures 5(a) and 5(b) demonstrate the viscosity and shear stress vs. shear rate curves of the bMSNs@DMA–MPC (1:4) aqueous suspensions with various concentrations (1, 2, and 5 mg/mL). Within the tested range of shear rate, the shear stress is proportional to the shear rate, and it gradually becomes higher with the increase in the concentration. Similarly, the viscosity presents a slightly increasing tendency with the increase in the concentration as well.

The lubrication performance of the bMSNs@DMA–MPC aqueous suspensions with various mass ratios of the DMA–MPC copolymer (4:1, 1:1, and 1:4) is examined under various conditions including concentration, contact stress, and reciprocating frequency, and the results are shown in Figs. 5(c)–5(f). Figure 5(c) demonstrates the comparison of COF values between bMSNs and bMSNs@DMA–MPC at various concentrations (1, 2, and 5 mg/mL) under a contact stress of 22.1 MPa and a reciprocating frequency of 1 Hz. It is clear that the COF values of bMSNs@DMA–MPC are smaller than those of bMSNs, which becomes slightly larger with the increase in the concentration. This is considered to be attributed to the agglomeration of the nanoparticles under higher concentrations. Figure 5(d) illustrates the comparison of COF values between bMSNs and bMSNs@DMA–MPC at different contact stresses (15.4, 19.3, and 22.1 MPa) under a concentration of 1 mg/mL and a reciprocating frequency of 1 Hz. Clearly, the COF values of bMSNs@DMA–MPC are much lower than those of bMSNs, which are slightly reduced with the increase in contact stress. It should be noted that the COF values of bMSNs@DMA–MPC indicate a slight decreasing trend when the mass ratio of MPC in the DMA–MPC copolymer is higher, and the lowest value obtained from the tribological test is about 0.018 for bMSNs@DMA–MPC (1:4). Figure 5(e) displays the

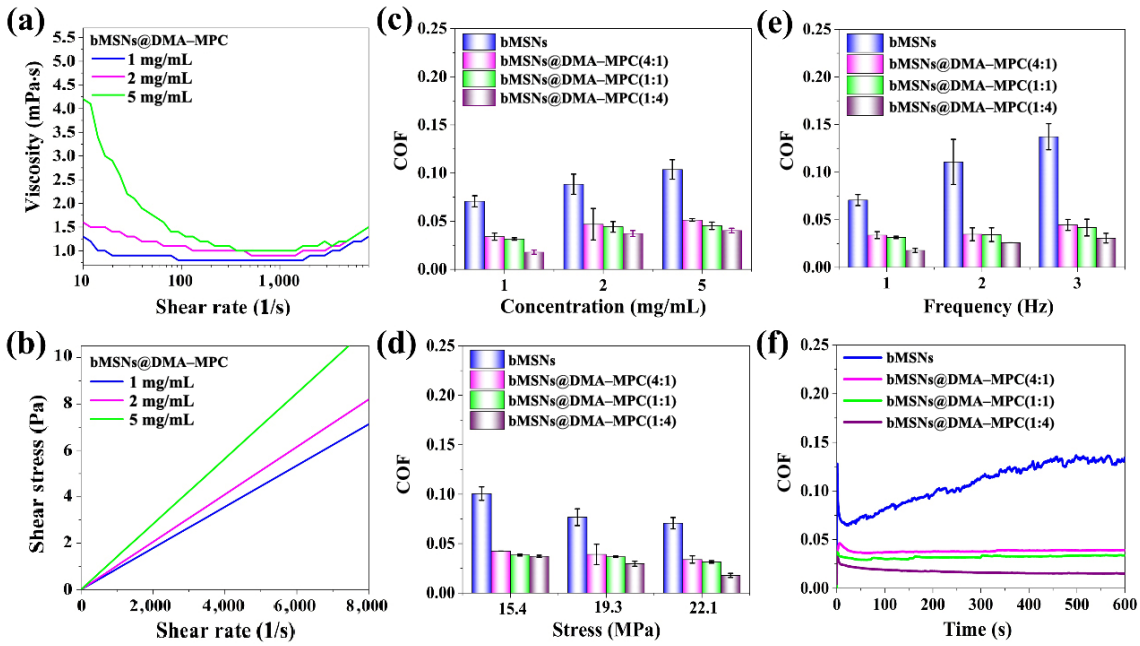

Fig. 5 Characterizations of the rheological properties and lubrication performances of the bMSNs and bMSNs@DMA–MPC nanoparticles under various experimental conditions: (a) viscosity vs. shear rate curve and (b) shear stress vs. shear rate curve for bMSNs@DMA–MPC (1:4) at the concentrations of 1, 2, and 5 mg/mL. COF values of bMSNs and bMSNs@DMA–MPC at different conditions: (c) concentration: 1, 2, and 5 mg/mL; contact stress: 22.1 MPa; and reciprocating frequency: 1 Hz; (d) contact stress: 15.4, 19.3, and 22.1 MPa; concentration: 1 mg/mL; and reciprocating frequency: 1 Hz; and (e) reciprocating frequency: 1, 2, and 3 Hz; concentration: 1 mg/mL; and contact stress: 22.1 MPa. (f) COF–time curves of bMSNs and bMSNs@DMA–MPC at a concentration of 1 mg/mL, a contact stress of 22.1 MPa, and a reciprocating frequency of 1 Hz.

comparison of COF values between bMSNs and bMSNs@DMA–MPC at various reciprocating frequencies (1, 2, and 3 Hz) under a concentration of 1 mg/mL and a contact stress of 22.1 MPa. Similarly, the COF values of bMSNs are larger with the increase in the reciprocating frequency, while the influence on bMSNs@DMA–MPC is not quite obvious. Figure 5(f) shows the COF vs. time plots of bMSNs and bMSNs@DMA–MPC at the concentration of 1 mg/mL, the contact stress of 22.1 MPa, and the reciprocating frequency of 1 Hz. Compared with bMSNs, which present a gradually increasing trend, the plots of bMSNs@DMA–MPC are very stable, indicating that bMSNs@DMA–MPC aqueous suspensions may be used as an effective biolubricant to reduce interfacial friction. The lubrication mechanism of bMSNs@DMA–MPC is owing to the hydrated lubrication of the phosphorylcholine groups in the DMA–MPC copolymer on the surface of the nanoparticles. Specifically, many free water molecules can surround the phosphorylcholine groups and then form a strong hydration shell owing to the interactions between the water dipole and enclosed charges. The hydration shell behaves in a fluidlike response under shear, and correspondingly greatly enhances interfacial lubrication between two sliding surfaces [22].

The lubrication performance of the bMSNs and bMSNs@DMA–MPC nanoparticles with an extended time duration (contact pressure: 22.1 MPa; reciprocating frequency: 1 Hz; and concentration: 1 mg/mL) is displayed in Fig. 6(a). It is clear from the COF vs. time plot that the COF value of bMSNs shows a gradually increasing trend, while the plot of bMSNs@DMA–MPC (1:4) is stable with a relatively lower COF value of 0.018. The surface morphology of the wear zone on the Ti6Al4V surface is examined using an optical interferometer, and the results are demonstrated in Figs. 6(b)–6(e). The scratch on the Ti6Al4V surface using bMSNs@DMA–MPC (1:4) shows a significant reduction in both wear width and depth (47.54 and 0.265 μm) than that of bMSNs (170.3 and 2.30 μm). This indicates that the bMSNs@DMA–MPC nanoparticles can effectively reduce surface wear under mechanical friction. Figure 6(f) presents the comparison of lubrication properties for the bMSNs and bMSNs@DMA–MPC nanoparticles incubated with SBF at different time intervals. The results indicate that with the increase in the degradation time, the

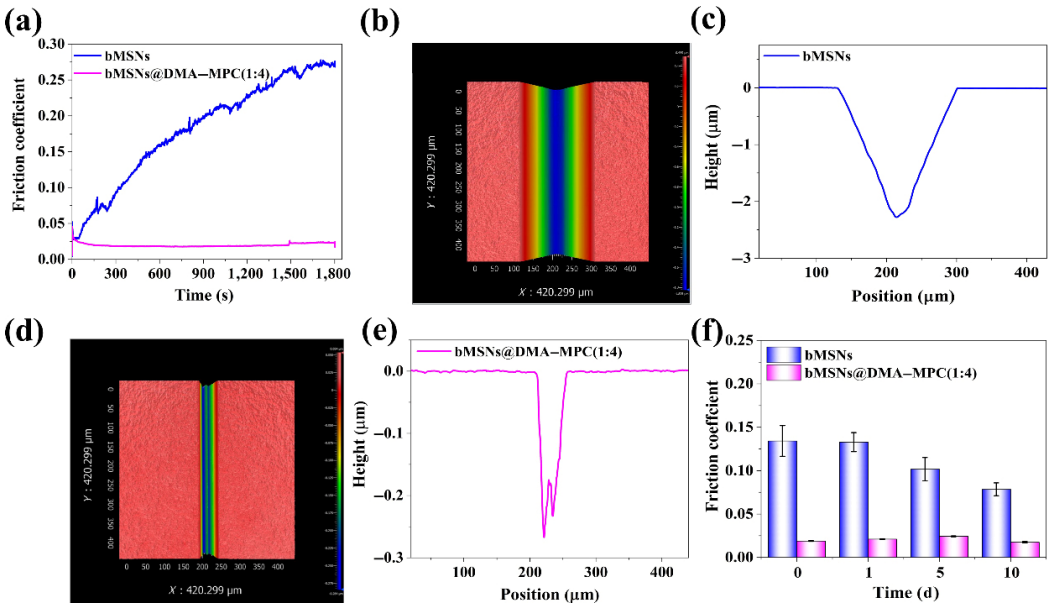

Fig. 6 Characterizations of the lubrication properties of the bMSNs and bMSNs@DMA–MPC nanoparticles with extended time duration and biodegradation test conditions. (a) COF–time plots of bMSNs and bMSNs@DMA–MPC at a concentration of 1 mg/mL, a contact stress of 22.1 MPa, a reciprocating frequency of 1 Hz, and a duration of 30 min. Surface morphologies of the wear zone on the Ti6Al4V surface and the corresponding surface profiles across the wear scratches for (b, c) bMSNs and (d, e) bMSNs@DMA–MPC nanoparticles. (f) COF values of the bMSNs and bMSNs@DMA–MPC nanoparticles incubated with SBF at different time intervals. Tribological test conditions are contact pressure: 22.1 MPa; concentration: 1 mg/mL; reciprocating frequency: 1 Hz; and time: 10 min.

average COF values of bMSNs@DMA–MPC (1:4) (0 d: 0.018; 1 d: 0.021; 5 d: 0.024; 10 d: 0.017) are much lower than that of bMSNs (0 d: 0.134; 1 d: 0.133; 5 d: 0.102; 10 d: 0.079). The decrease in the COF value of bMSNs is attributed to the progressive dissolution of bMSNs over time under physiological conditions. The bMSNs@DMA–MPC (1:4) nanoparticles maintain excellent lubrication performance during the whole biodegradation process, and the COF value does not change much, which is related with the hydration lubrication effect of the DMA–MPC coating modified on the surface of the nanoparticles.

3.4 *In vitro* drug release property

As a typical anti-inflammation drug, DS has been commonly used in previous studies for the treatment of osteoarthritis [54]. In the present study, DS is encapsulated into the bMSNs@DMA–MPC nanoparticles to achieve dual-functional properties of improved lubrication and local drug delivery. Figure 7(a) shows the standard curve of DS measured in PBS. It is calculated from the fitted equation of the standard curve that the LC and EE of bMSNs@DMA–MPC (1:4) are 8.8% and 54.7%, respectively, which are higher than those of bMSNs (5.6% and 35.0%). This result may be attributed to the interaction between the drug molecule and the DMA–MPC copolymer on the surface of the nanoparticles. Figure 7(b) exhibits the drug release curves of the drug-loaded nanoparticles, i.e., bMSNs–DS and bMSNs@DMA–MPC–DS. Clearly, bMSNs@DMA–MPC–DS prensents a sustained drug release behavior, and the amount of released drug is significantly smaller than that of bMSNs–DS. After 80 h, the cumulative drug release of bMSNs–DS is 70.5%, which is much higher than that of bMSNs@DMA–MPC–DS (39.1%).

3.5 *In vitro* biodegradation property

Biodegradability of implanted nanomaterials has received considerable attention from the researchers as a prerequisite for clinical applications [55]. To investigate the *in vitro* biodegradation property of the nanoparticles, bMSNs and bMSNs@DMA–MPC (1:4) are incubated in SBF at 37 °C for different time durations until 10 d. The TEM result of the nanoparticles is shown in Fig. 8, and it is clear that the biodegradation behavior of the two nanoparticles is similar. Specifically, the morphologies of the nanoparticles are almost unchanged at day 1. However, significant biodegradation of the nanoparticles is observed at day 5 with an obvious reduction in the nanoparticle size. At day 10, the size of the nanoparticles becomes even smaller, and only a few remaining fragments can be detected. The above result indicates that the bMSNs@DMA–MPC nanoparticles can be completely biodegraded within 10 d when being incubated in SBF *in vitro*, which is considered to be beneficial for biomedical applications to avoid accumulation *in vivo*.

3.6 *In vitro* cell cytotoxicity

Biocompatibility is another important matter of concern for implanted nanomaterials, and therefore the *in vitro* cytotoxicity test of the bMSNs and bMSNs@DMA–MPC (1:4) nanoparticles is performed using MC3T3-E1 cells based on the live/dead staining assay and CCK-8 assay. Figure 9(a) demonstrates the results of live/dead staining assay for these nanoparticles at a concentration of 0.05 mg/mL,

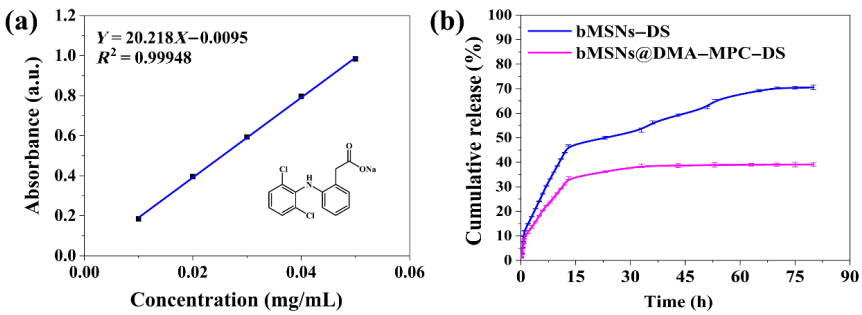

Fig. 7 *In vitro* drug release of the bMSNs and bMSNs@DMA–MPC (1:4) nanoparticles. (a) Standard curve of DS with different concentrations (0.01, 0.02, 0.03, 0.04, and 0.05 mg/mL) measured in PBS. (b) Drug release profiles of the nanoparticles in the PBS at 25 °C for 80 h.

following incubation with the cells for 1, 3, and 5 d. The MC3T3-E1 cells are metabolically active, and few dead cells are detected at various time durations. Figures 9(b) and 9(c) show the results of CCK-8 assay for the nanoparticles with various concentrations (0.05–1.0 mg/mL) and different time durations (1, 3, and 5 d). Under all the test conditions, the cellular activity is above 80%, and no significant differences are observed among the experimental groups. The results of CCK-8 as well as live/dead staining assays indicate that the nanoparticles have no significant cytotoxicity to the MC3T3-E1 cells.

3.7 Anti-inflammation property

The anti-inflammation property of the drug-loaded nanoparticles is evaluated based on a preliminary test to determine whether the nanoparticles can be used for the treatment of osteoarthritis. The inflammation factors, such as IL-6 and IL-1β, have been shown to be closely associated with the development of osteoarthritis, and LPS can induce the macrophages to secrete these pro-inflammatory cytokines [56]. In the present study, the activated macrophages by LPS are incubated with bMSNs,

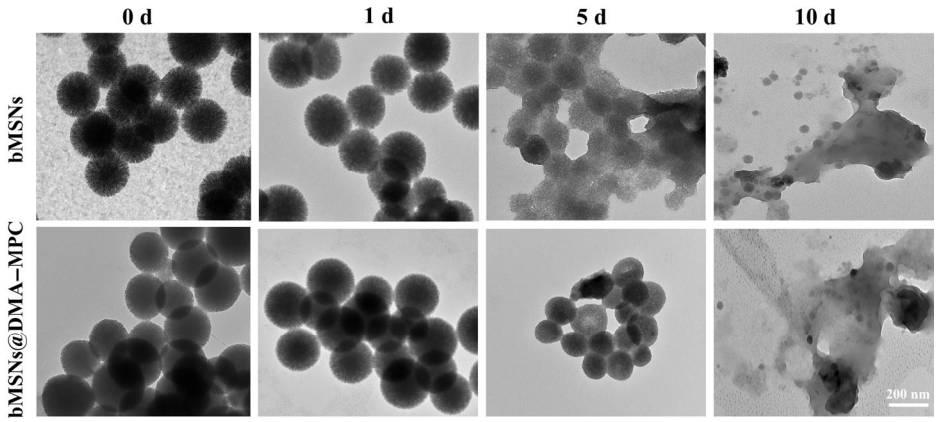

Fig. 8 Representative TEM images for the characterization of biodegradation properties of the bMSNs and bMSNs@DMA–MPC (1:4) nanoparticles incubated in SBF at 37 °C.

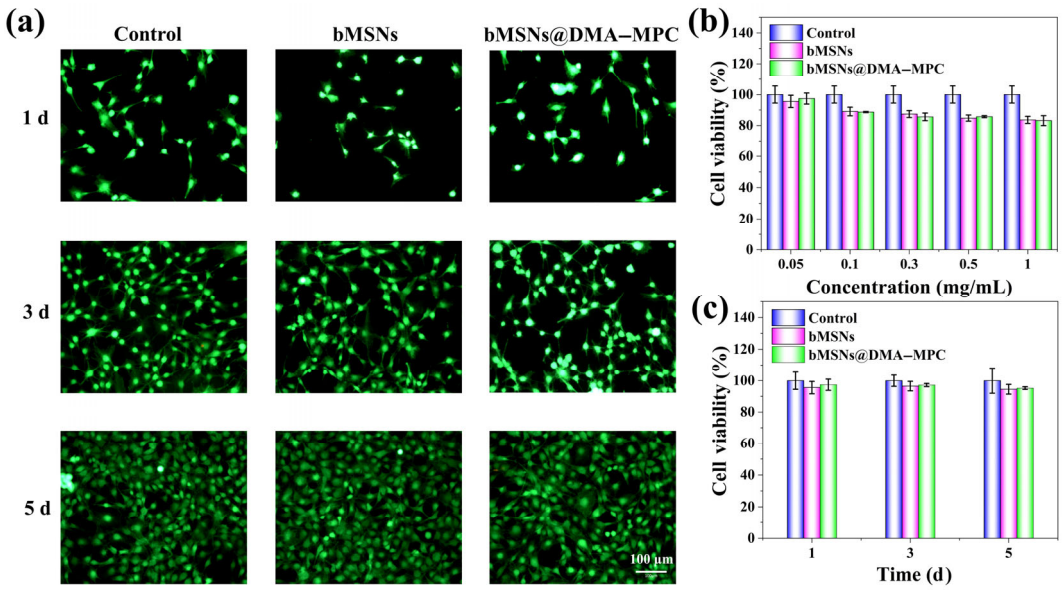

Fig. 9 *In vitro* cell cytotoxicity evaluation of the bMSNs and bMSNs@DMA–MPC (1:4) nanoparticles. (a) Representative laser scanning confocal microscopy images showing the MC3T3-E1 cells incubated with the nanoparticles for 1, 3, and 5 d, as determined by the live/dead staining assay. CCK-8 assay result showing cell viability of the MC3T3-E1 cells incubated with the nanoparticles at (b) different concentrations and (c) different time durations.

bMSNs@DMA–MPC (1:4), bMSNs–DS, and bMSNs@DMA–MPC (1:4)–DS for 24 h, and the levels of IL-1β and IL-6 determined by the ELISA kit are displayed in Figs. 10(a) and 10(b). It is clear that the trends of two inflammatory factors are similar, where the incubation with the drug-loaded nanoparticles, i.e., bMSNs–DS and bMSNs@DMA–MPC (1:4)–DS, significantly down-regulates the expression levels. However, there are almost no anti-inflammation effects for the nanoparticles of bMSNs and bMSNs@DMA–MPC (1:4). It is exhibited that the anti-inflammation effect of bMSNs@DMA–MPC (1:4)–DS is even better than bMSNs–DS, which may be related with the higher drug LC and also sustained drug release performance.

4 Conclusions

In the present study, a biomimetic self-adhesive copolymer of DMA–MPC was prepared via free radical polymerization, which was coated onto the surface of bMSNs to prepare dual-functional nanoparticles, i.e., bMSNs@DMA–MPC–DS, with improved lubrication and local sustained drug release for treating the early-stage osteoarthritis. The surface characterizations including the TEM, FTIR, TGA, XPS, etc., indicated that the DMA–MPC copolymer was modified successfully on the surface of the nanoparticles using a simple dip-coating method. The tribological test indicated that the lubrication performance of the bMSNs@DMA–MPC nanoparticles was significantly improved in comparison with bMSNs, which was mainly owing to the hydration lubrication of the phosphorylcholine groups in the DMA–MPC copolymer. The *in vitro* drug release test displayed that the drug-loaded bMSNs@DMA–MPC–DS nanoparticles were endowed with a sustained drug release performance. In addition, the *in vitro* biological tests demonstrated that the dual-functional nanoparticles were biodegradable and biocompatible, and could down-regulate the expression levels of typical inflammation factors including IL-1β and IL-6. In conclusion, the bioinspired dual-functional nanoparticles with the properties of improved lubrication and sustained drug release developed herein might be a potential intra-articular injected biolubricant for early-stage osteoarthritis treatment.

Acknowledgements

This study was financially supported by the National Natural Science Foundation of China (52022043 and 21868011), Tsinghua University–Peking Union Medical College Hospital Initiative Scientific Research Program (20191080593), Precision Medicine Foundation, Tsinghua University, China (10001020107), the National Key R&D Program of China (2017YFC1103800), and Research Fund of State Key Laboratory of Tribology, Tsinghua University, China (SKLT2022C18).

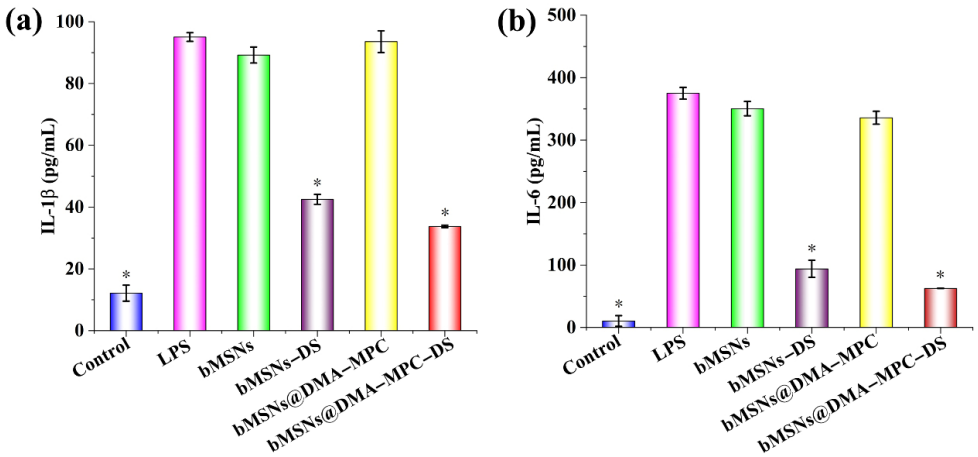

Fig. 10 Anti-inflammation properties of the drug-loaded nanoparticles characterized by incubating the activated macrophages with the same concentration of bMSNs, bMSNs–DS, bMSNs@DMA–MPC (1:4), and bMSNs@DMA–MPC (1:4)–DS for a duration of 24 h. The expression levels of inflammation factors including (a) IL-1β and (b) IL-6 are measured using the ELISA kit. ($n = 3$, $^{*}P < 0.05$, for comparison with the LPS group).

References

[1] Klein J. Repair or replacement: A joint perspective. *Science* **323**(5910): 47–48 (2009)

[2] Wang Y X, Sun Y L, Avestro A J, McGonigal P R, Zhang H Y. Supramolecular repair of hydration lubrication surfaces. *Chem* **8**(2): 480–493 (2022)

[3] Morgese G, Trachsel L, Romio M, Divandari M, Ramakrishna S N, Benetti E M. Topological polymer chemistry enters surface science: Linear versus cyclic polymer brushes. *Angew Chem Int Ed* **55**(50): 15583–15588 (2016)

[4] Morgese G, Cavalli E, Rosenboom J G, Zenobi-Wong M, Benetti E M. Cyclic polymer grafts that lubricate and protect damaged cartilage. *Angew Chem Int Ed* **57**(6): 1621–1626 (2018)

[5] Xie R J, Yao H, Mao A S, Zhu Y, Qi D W, Jia Y G, Gao M, Chen Y H, Wang L, Wang D A, et al. Biomimetic cartilage-lubricating polymers regenerate cartilage in rats with early osteoarthritis. *Nat Biomed Eng* **5**(10): 1189–1201 (2021)

[6] Kosinska M K, Ludwig T E, Liebisch G, Zhang R Y, Siebert H C, Wilhelm J, Kaesser U, Dettmeyer R B, Klein H, Ishaque B, et al. Articular joint lubricants during osteoarthritis and rheumatoid arthritis display altered levels and molecular species. *PLoS One* **10**(5): e0125192 (2015)

[7] Ludwig T E, McAllister J R, Lun V, Wiley J P, Schmidt T A. Diminished cartilage-lubricating ability of human osteoarthritic synovial fluid deficient in proteoglycan 4: Restoration through proteoglycan 4 supplementation. *Arthritis Rheum* **64**(12): 3963–3971 (2012)

[8] Morgese G, Benetti E M, Zenobi-Wong M. Molecularly engineered biolubricants for articular cartilage. *Adv Healthc Mater* **7**(16): 1701463 (2018)

[9] Poulet B, Staines K A. New developments in osteoarthritis and cartilage biology. *Curr Opin Pharmacol* **28**: 8–13 (2016)

[10] Szychlinska M A, Leonardi R, Al-Qahtani M, Mobasheri A, Musumeci G. Altered joint tribology in osteoarthritis: Reduced lubricin synthesis due to the inflammatory process. New horizons for therapeutic approaches. *Ann Phys Rehabil Med* **59**(3): 149–156 (2016)

[11] Yan X, Yang B, Chen Y R, Song Y F, Ye J, Pan Y F, Zhou B N, Wang Y Q, Mao F B, Dong Y C, et al. Anti-friction MSCs delivery system improves the therapy for severe osteoarthritis. *Adv Mater* **33**(52): 2104758 (2021)

[12] Kloppenburg M, Berenbaum F. Osteoarthritis year in review 2019: Epidemiology and therapy. *Osteoarthr Cartil* **28**(3): 242–248 (2020)

[13] Sun T, Sun Y L, Zhang H Y. Phospholipid-coated mesoporous silica nanoparticles acting as lubricating drug nanocarriers. *Polymers* **10**(5): 513 (2018)

[14] Jones G, Winzenberg T. Osteoarthritis: A new short-term treatment option? *Lancet* **394**(10213): 1967–1968 (2019)

[15] Rothenfluh D A, Bermudez H, O'Neil C P, Hubbell J A. Biofunctional polymer nanoparticles for intra-articular targeting and retention in cartilage. *Nat Mater* **7**(3): 248–254 (2008)

[16] Jones I A, Togashi R, Wilson M L, Heckmann N, Vangsness C T Jr. Intra-articular treatment options for knee osteoarthritis. *Nat Rev Rheumatol* **15**(2): 77–90 (2019)

[17] Chen H, Sun T, Yan Y F, Ji X L, Sun Y L, Zhao X, Qi J, Cui W G, Deng L F, Zhang H Y. Cartilage matrix-inspired biomimetic superlubricated nanospheres for treatment of osteoarthritis. *Biomaterials* **242**: 119931 (2020)

[18] Lin W F, Klein J. Recent progress in cartilage lubrication. *Adv Mater* **33**(18): 2005513 (2021)

[19] Liu G Q, Liu Z L, Li N, Wang X L, Zhou F, Liu W M. Hairy polyelectrolyte brushes-grafted thermosensitive microgels as artificial synovial fluid for simultaneous biomimetic lubrication and arthritis treatment. *ACS Appl Mater Interfaces* **6**(22): 20452–20463 (2014)

[20] Morgese G, Cavalli E, Müller M, Zenobi-Wong M, Benetti E M. Nanoassemblies of tissue-reactive, polyoxazoline graft-copolymers restore the lubrication properties of degraded cartilage. *ACS Nano* **11**(3): 2794–2804 (2017)

[21] Seror J, Merkher Y, Kampf N, Collinson L, Day A J, Maroudas A, Klein J. Normal and shear interactions between hyaluronan–aggrecan complexes mimicking possible boundary lubricants in articular cartilage in synovial joints. *Biomacromolecules* **13**(11): 3823–3832 (2012)

[22] Klein J. Hydration lubrication. *Friction* **1**(1): 1–23 (2013)

[23] Kankala R K, Han Y H, Na J, Lee C H, Sun Z Q, Wang S B, Kimura T, Ok Y S, Yamauchi Y, Chen A Z, et al. Nanoarchitectured structure and surface biofunctionality of mesoporous silica nanoparticles. *Adv Mater* **32**(23): 1907035 (2020)

[24] Mora-Raimundo P, Lozano D, Benito M, Mulero F, Manzano M, Vallet-Regí M. Osteoporosis remission and new bone formation with mesoporous silica nanoparticles. *Adv Sci* **8**(16): 2101107 (2021)

[25] Yu M H, Jambhrunkar S, Thorn P, Chen J Z, Gu W Y, Yu C Z. Hyaluronic acid modified mesoporous silica nanoparticles for targeted drug delivery to CD44-overexpressing cancer cells. *Nanoscale* **5**(1): 178–183 (2013)

[26] Zhang K, Yang J L, Sun Y L, He M R, Liang J, Luo J, Cui W G, Deng L F, Xu X Y, Wang B, et al. Thermo-sensitive dual-functional nanospheres with enhanced lubrication and drug delivery for the treatment of osteoarthritis. *Chem Eur J* **26**(46): 10564–10574 (2020)

[27] Zheng Y W, Yang J L, Liang J, Xu X Y, Cui W G, Deng L F, Zhang H Y. Bioinspired hyaluronic acid/phosphorylcholine polymer with enhanced lubrication and anti-inflammation. *Biomacromolecules* **20**(11): 4135–4142 (2019)

[28] Wan L, Wang Y, Tan X L, Sun Y L, Luo J, Zhang H Y. Biodegradable lubricating mesoporous silica nanoparticles for osteoarthritis therapy. *Friction* **10**(1): 68–79 (2022)

[29] Tan X L, Sun Y L, Sun T, Zhang H Y. Mechanised lubricating silica nanoparticles for on-command cargo release on simulated surfaces of joint cavities. *Chem Commun* **55**(18): 2593–2596 (2019)

[30] Ishihara K, Ito M, Fukazawa K, Inoue Y. Interface of phospholipid polymer grafting layers to analyze functions of immobilized oligopeptides involved in cell adhesion. *ACS Biomater Sci Eng* **6**(7): 3984–3993 (2020)

[31] Yang J L, Han Y, Lin J W, Zhu Y, Wang F, Deng L F, Zhang H Y, Xu X Y, Cui W G. Ball-bearing-inspired polyampholyte-modified microspheres as bio-lubricants attenuate osteoarthritis. *Small* **16**(44): 2004519 (2020)

[32] Lee H, Dellatore S M, Miller W M, Messersmith P B. Mussel-inspired surface chemistry for multifunctional coatings. *Science* **318**(5849): 426–430 (2007)

[33] Han Y, Liu S Z, Sun Y L, Gu Y H, Zhang H Y. Bioinspired surface functionalization of titanium for enhanced lubrication and sustained drug release. *Langmuir* **35**(20): 6735–6741 (2019)

[34] He Y, Xu L H, Feng X, Zhao Y P, Chen L. Dopamine-induced nonionic polymer coatings for significantly enhancing separation and antifouling properties of polymer membranes: Codeposition versus sequential deposition. *J Membr Sci* **539**: 421–431 (2017)

[35] Shen D K, Yang J P, Li X M, Zhou L, Zhang R Y, Li W, Chen L, Wang R, Zhang F, Zhao D Y. Biphase stratification approach to three-dimensional dendritic biodegradable mesoporous silica nanospheres. *Nano Lett* **14**(2): 923–932 (2014)

[36] Jiao Y Y, Liu S Z, Sun Y L, Yue W, Zhang H Y. Bioinspired surface functionalization of nanodiamonds for enhanced lubrication. *Langmuir* **34**(41): 12436–12444 (2018)

[37] Zhao W W, Wang H, Wang H M, Han Y, Zheng Z B, Liu X D, Feng B, Zhang H Y. Light-responsive dual-functional biodegradable mesoporous silica nanoparticles with drug delivery and lubrication enhancement for the treatment of osteoarthritis. *Nanoscale* **13**(13): 6394–6399 (2021)

[38] Guo S B, Yu B, Ahmed A, Cong H L, Shen Y Q. Synthesis of polyacrylonitrile/polytetrahydropyrimidine (PAN/PTHP) nanofibers with enhanced antibacterial and anti-viral activities for personal protective equipment. *J Hazard Mater* **424**: 127602 (2022)

[39] Tong X, Zhang D C, Zhang X T, Su Y C, Shi Z M, Wang K, Lin J G, Li Y C, Lin J X, Wen C E. Microstructure, mechanical properties, biocompatibility, and *in vitro* corrosion and degradation behavior of a new Zn–5Ge alloy for biodegradable implant materials. *Acta Biomater* **82**: 197–204 (2018)

[40] Zhao Y Y, Wei C F, Chen X, Liu J W, Yu Q Q, Liu Y N, Liu J. Drug delivery system based on near-infrared light-responsive molybdenum disulfide nanosheets controls the high-efficiency release of dexamethasone to inhibit inflammation and treat osteoarthritis. *ACS Appl Mater Interfaces* **11**(12): 11587–11601 (2019)

[41] Yang L, Sun L Y, Zhang H, Bian F K, Zhao Y J. Ice-inspired lubricated drug delivery particles from microfluidic electrospray for osteoarthritis treatment. *ACS Nano* **15**(12): 20600–20606 (2021)

[42] Zhao W W, Wang H, Han Y, Wang H M, Sun Y L, Zhang H Y. Dopamine/phosphorylcholine copolymer as an efficient joint lubricant and ROS scavenger for the treatment of osteoarthritis. *ACS Appl Mater Interfaces* **12**(46): 51236–51248 (2020)

[43] Ma M, Huang Y, Chen H R, Jia X Q, Wang S G, Wang Z Z, Shi J L. Bi_2S_3-embedded mesoporous silica nanoparticles for efficient drug delivery and interstitial radiotherapy sensitization. *Biomaterials* **37**: 447–455 (2015)

[44] Chatterjee S, Ohshio M, Yusa S-i, Ooya T. Controlled

micelle formation and stable capture of hydrophobic drug by alkylated POSS methacrylate block copolymers. *ACS Appl Polym Mater* **1**(8): 2108–2119 (2019)

[45] Chen Z W, Li Z H, Lin Y H, Yin M L, Ren J S, Qu X G. Bioresponsive hyaluronic acid-capped mesoporous silica nanoparticles for targeted drug delivery. *Chem Eur J* **19**(5): 1778–1783 (2013)

[46] Xu X Y, Li H R, Li K, Zeng Q, Liu Y, Zeng Y, Chen D, Liang J M, Chen X L, Zhan Y H. A photo-triggered conjugation approach for attaching RGD ligands to biodegradable mesoporous silica nanoparticles for the tumor fluorescent imaging. *Nanomed Nanotechnol Biol Med* **19**: 136–144 (2019)

[47] Vatankhah-Varnosfaderani M, Hu X B, Li Q X, Adelnia H, Ina M, Sheiko S S. Universal coatings based on zwitterionic–dopamine copolymer microgels. *ACS Appl Mater Interfaces* **10**(24): 20869–20875 (2018)

[48] Niu J Q, Wang H H, Chen J, Chen X Q, Han X, Liu H L. Bio-inspired zwitterionic copolymers for antifouling surface and oil–water separation. *Colloids Surf A Physicochem Eng Aspects* **626**: 127016 (2021)

[49] Varache M, Bezverkhyy I, Weber G, Saviot L, Chassagnon R, Baras F, Bouyer F. Loading of cisplatin into mesoporous silica nanoparticles: Effect of surface functionalization. *Langmuir* **35**(27): 8984–8995 (2019)

[50] Yan Y F, Sun T, Zhang H B, Ji X L, Sun Y L, Zhao X, Deng L F, Qi J, Cui W G, Santos H A, et al. *Euryale ferox* seed-inspired superlubricated nanoparticles for treatment of osteoarthritis. *Adv Funct Mater* **29**(4): 1807559 (2019)

[51] Liu S H, Zhao X, Tang J M, Han Y M, Lin Q K. Drug-eluting hydrophilic coating modification of intraocular lens via facile dopamine self-polymerization for posterior capsular opacification prevention. *ACS Biomater Sci Eng* **7**(3): 1065–1073 (2021)

[52] Valle-Delgado J J, Johansson L S, Österberg M. Bioinspired lubricating films of cellulose nanofibrils and hyaluronic acid. *Colloids Surf B Biointerfaces* **138**: 86–93 (2016)

[53] Mancipe Castro L M, Sequeira A, García A J, Guldberg R E. Articular cartilage- and synoviocyte-binding poly(ethylene glycol) nanocomposite microgels as intra-articular drug delivery vehicles for the treatment of osteoarthritis. *ACS Biomater Sci Eng* **6**(9): 5084–5095 (2020)

[54] Martel-Pelletier J, Barr A J, Cicuttini F M, Conaghan P G, Cooper C, Goldring M B, Goldring S R, Jones G, Teichtahl A J, Pelletier J P. Osteoarthritis. *Nat Rev Dis Primers* **2**: 16072 (2016)

[55] Nadarassan D, Loni A, Canham L T, Scoutaris N, Trivedi V, Douroumis D. Ultrahigh nanostructured drug payloads from degradable mesoporous silicon aerocrystals. *Int J Pharm* **607**: 120840 (2021)

[56] Liu M, Xie Z K, Sun G, Chen L J, Qi D K, Zhang H W, Xiong J Y, Furey A, Rahman P, Lei G H, et al. Macrophage migration inhibitory factor may play a protective role in osteoarthritis. *Arthritis Res Ther* **23**: 59 (2021)

Xiaowei MAO. He received his B.S. in chemical engineering and technology from Jinggangshan University, China, in 2018. He is currently a joint graduate student in Tsinghua University, China. His research interests include biotribology and drug delivery materials.

Kexin CHEN. She graduated from Tianjin Medical University, China, in 2019. She is currently a graduate student at Peking University School of Nursing, China. Her research interest is biomedical materials and devices for oral applications.

Yuguang WANG. He received his Ph.D. at Peking University School and Hospital of Stomatology, China, in 2009. He was a visiting scholar of Massachusetts General Hospital, Harvard University, USA, in 2015. He is currently an associate professor at the Center of Digital Dentistry, China. His research interest is laser technology and light-responsive materials for oral applications.

Bo WANG. He received his B.S. and Ph.D. degrees from Hainan University, China and Zhejiang University, China, respectively. He is a professor at the College of Chemical and Biological Engineering, Shandong University of Science and Technology, China. His research covers green chemistry, bio-catalysis, and asymmetric synthesis.

Hongyu ZHANG. He received his B.S. in Tianjin University, China (2005) and Ph.D. in University of Huddersfield, UK (2009). He is an associate professor at the State Key Laboratory of Tribology, Department of Mechanical Engineering, Tsinghua University, China. His research interests focus on the development of lubricating biomaterials such as nanoparticles, coatings, hydrogels, and electrospun nanofibers, which integrate the multi-disciplinary knowledge including biotribology, chemistry, materials science, and medicine to address clinical issues, e.g., osteoarthritis, anti-tissue/cell/bacteria adhesion, bone tissue engineering, etc.